Article

Cell Reports

Chromatin Architecture of the Pitx2 Locus Requires CTCF- and Pitx2-Dependent Asymmetry that Mirrors Embryonic Gut Laterality

Graphical Abstract

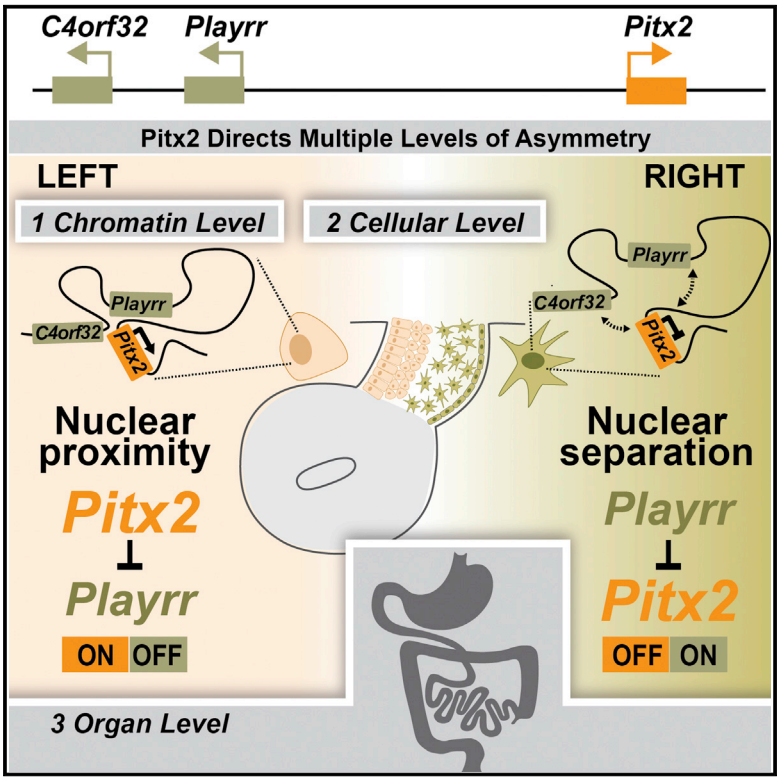

Authors

Ian C. Welsh, Hojoong Kwak, Frances L. Chen, ..., Min Zhang, James F. Martin, Natasza A. Kurpios

Correspondence

nk378@cornell.edu

In Brief

Asymmetric expression of the homeobox transcription factor *Pitx2* patterns LR organ morphogenesis. Welsh et al. identify LR asymmetric gene expression from the *Pitx2* locus and establish an in vivo model to dissect long-range *cis*-regulatory interactions and the role of chromatin topology in asymmetric gene expression.

Highlights

- *Pitx2* expression is mirrored by right-specific expression of adjacent genes at the *Pitx2* locus
- Pitx2 represses left-side expression of a conserved lncRNA called *Playrr*
- *Playrr* functions in vivo to repress *Pitx2* expression
- *Pitx2*/*Playrr* antagonism is mirrored by LR chromatin topology

Accession Numbers

GSE71117

Welsh et al., 2015, Cell Reports *13*, 337–349
October 13, 2015 ©2015 The Authors
http://dx.doi.org/10.1016/j.celrep.2015.08.075

Cell Reports
Article

Chromatin Architecture of the Pitx2 Locus Requires CTCF- and Pitx2-Dependent Asymmetry that Mirrors Embryonic Gut Laterality

Ian C. Welsh,[1] Hojoong Kwak,[2] Frances L. Chen,[1] Melissa Werner,[1] Lindsay S. Shopland,[3,4] Charles G. Danko,[5] John T. Lis,[2] Min Zhang,[6] James F. Martin,[6,7,8,9] and Natasza A. Kurpios[1,*]
[1]Department of Molecular Medicine, College of Veterinary Medicine, Cornell University, Ithaca, NY 14853, USA
[2]Department of Molecular Biology and Genetics, Cornell University, Ithaca, NY 14853, USA
[3]The Jackson Laboratory, Bar Harbor, ME, 04609, USA
[4]Eastern Maine Medical Center Cancer Care, 33 Whiting Hill Road, Brewer, ME 04412, USA
[5]Department of Biomedical Sciences, The Baker Institute for Animal Health, Cornell University, Ithaca, NY 14853, USA
[6]Department of Molecular Physiology and Biophysics, Baylor College of Medicine, Houston, TX 77030, USA
[7]Texas Heart Institute, Houston, TX 77030, USA
[8]Program in Developmental Biology, Baylor College of Medicine, Houston, TX 77030, USA
[9]Cardiovascular Research Institute, Baylor College of Medicine, Houston, TX 77030, USA
*Correspondence: nk378@cornell.edu
http://dx.doi.org/10.1016/j.celrep.2015.08.075

SUMMARY

Expression of Pitx2 on the left side of the embryo patterns left-right (LR) organs including the dorsal mesentery (DM), whose asymmetric cell behavior directs gut looping. Despite the importance of organ laterality, chromatin-level regulation of Pitx2 remains undefined. Here, we show that genes immediately neighboring *Pitx2* in chicken and mouse, including a long noncoding RNA (*Pitx2* locus-asymmetric regulated RNA or *Playrr*), are expressed on the right side and repressed by *Pitx2*. CRISPR/Cas9 genome editing of *Playrr,* 3D fluorescent in situ hybridization (FISH), and variations of chromatin conformation capture (3C) demonstrate that mutual antagonism between *Pitx2* and *Playrr* is coordinated by asymmetric chromatin interactions dependent on Pitx2 and CTCF. We demonstrate that transcriptional and morphological asymmetries driving gut looping are mirrored by chromatin architectural asymmetries at the *Pitx2* locus. We propose a model whereby Pitx2 auto-regulation directs chromatin topology to coordinate LR transcription of this locus essential for LR organogenesis.

INTRODUCTION

The external symmetry of vertebrates conceals left-right (LR) asymmetries of the internal organs essential for function and placement within the body cavity. LR patterning initiates early during gastrulation via transient signaling by Nodal, which yields persistent expression of the transcription factor Pitx2 throughout the left lateral mesoderm (Logan et al., 1998; Shiratori et al., 2001). *Pitx2* then specifies left identity within individual organ primordia. The control of laterality by *Pitx2* is very conserved, functioning even in basal deuterostomes such as sea urchin and non-bilaterians such as hydra (Duboc et al., 2005; Watanabe et al., 2014).

Regulation of *Pitx2* in vertebrates involves multiple isoforms. The *Pitx2a* and *2b* splice variants are expressed bilaterally, while *Pitx2c* is transcribed from a separate promoter and is exclusively left sided (Shiratori et al., 2006; Liu et al., 2001). *Pitx2*-null embryos die mid-gestation with global laterality defects (Lu et al., 1999). Moreover, *PITX2* is mutated in humans with Axenfeld-Rieger syndrome (ARS), characterized by mental retardation, craniofacial and body wall defects, and umbilical hernias (Semina et al., 1996). Importantly, some ARS patients bear no mutations in *Pitx2* coding sequences, but harbor lesions within a conserved gene desert adjacent to *PITX2*, suggesting *cis*-regulatory elements (*cis*-REs) within the desert are essential for *Pitx2* expression (Flomen et al., 1998; Volkmann et al., 2011; Reis et al., 2012). Furthermore, SNPs associated with *PITX2*-linked atrial fibrillation (AF) map to the same gene desert (Lubitz et al., 2010; Kent et al., 2002). Despite much available knowledge of early laterality control, specific genomic mechanisms governing the expression of its master effector gene remain unexplored.

Here we employ the unique binary (L versus R) organization of the gut dorsal mesentery (DM), a suspensory mesodermal bridge with asymmetries directed by left-sided *Pitx2* (Figure 1A, top). Condensation of the left side and expansion of the right side cause the DM to deform, tilting the attached gut tube leftward (Davis et al., 2008; Kurpios et al., 2008). This tilt biases asymmetric gut rotation, the disruption of which randomizes gut looping (Davis et al., 2008; Figure 1A, top).

To define the molecular composition of the DM, we laser dissected and microarray profiled the left (*Pitx2*-positive) and right (*Pitx2*-negative) sides of the DM when these asymmetries were apparent (chicken HH21, akin to mouse embryonic day

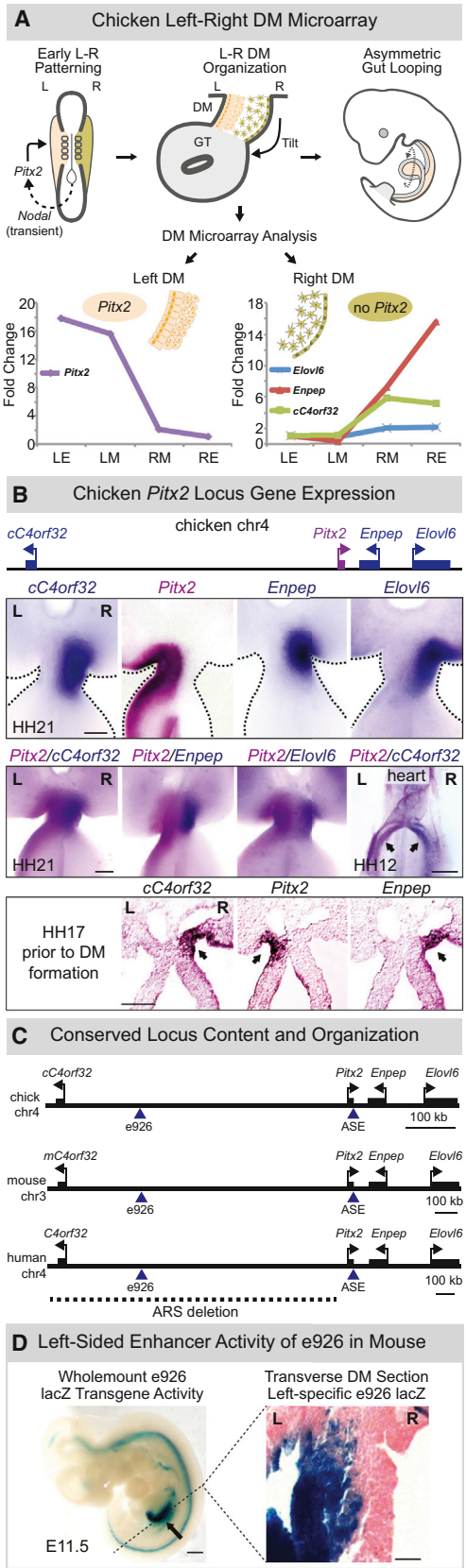

Figure 1. LR Asymmetric Gene Expression at the *Pitx2* Locus

(A and B) *Pitx2* initiates gut looping directed by LR changes in the DM cellular architecture (tan, left; green, right). (A) DM microarray (LE, left epithelium; LM, left mesenchyme; RM, right mesenchyme; RE, right epithelium) identifies genes linked to *Pitx2* with right-side-restricted expression, validated in (B) via whole-mount ISH (double-labeling *Pitx2*, magenta; right-specific genes, blue) at HH21 (DM), HH17 (lateral mesoderm, DM precursor, arrows), and HH12 (sinus venosus of the primitive heart, arrows).

(C) *Pitx2* locus conservation in chicken, mouse, and human (dashed line, human ARS deletion). Note human locus is inverted relative to its orientation on chr4.

(D) e926 directs left-specific reporter gene expression (LacZ) in the left DM of transgenic mouse embryos. Scale bars, 100 μm, HH21 and HH17 (B); 500 μm, HH12 (B); 500 μm, whole mount (D); and 25 μm, section (D). See also Figure S1.

[E]10.5) (Hamburger and Hamilton, 1951; Welsh et al., 2013). Here we reveal that genes neighboring *Pitx2* and the adjacent conserved gene desert are expressed in a right-specific pattern opposite to left-specific *Pitx2*. Within the gene desert, we identified a conserved sequence element e926 that functions endogenously as a promoter for a conserved long noncoding RNA (lncRNA) we named *Playrr*, which is exclusively transcribed in the right DM. Importantly, genetic analyses found that *Pitx2* expression and *Playrr* expression are mutually antagonistic. We employed fluorescent in situ hybridization (FISH) and variations of chromatin conformation capture (3C) to correlate this binary LR expression with nuclear architecture in the DM, and we identified conserved LR differences in nuclear proximity of e926/*Playrr* and *Pitx2* that are dependent on Pitx2 and CTCF. Our data demonstrate chromatin-level regulation that mirrors LR organogenesis and that tissue-specific *cis*-regulatory topology establishes LR transcription among higher vertebrates.

RESULTS

Right-Sided Expression of Genes at the *Pitx2* Locus Is Opposite to Pitx2 on the Left

Our previous microarray analysis of the left and right chicken DM (Welsh et al., 2013) aimed to identify *Pitx2* target effector genes responsible for cellular asymmetries in the DM. We first confirmed that *Pitx2* is the most differentially expressed gene on the left side of the DM, with ~19-fold higher expression in the left versus right DM (Figure 1A, graph). Our analyses also revealed that glutamyl aminopeptidase A (*Enpep*) is the most differentially expressed gene in the right DM, with ~17-fold higher expression (Figure 1A, graph). Remarkably, these two genes of highly contrasting transcription are located immediately adjacent to each other in the genome. Chicken *Pitx2* is flanked proximally by a large (~600-kb) gene desert and 27 kb distally by the convergently transcribed *Enpep* (Figure 1B). We confirmed these findings in situ and demonstrated that DM tissue asymmetry is mirrored by exclusive LR expression patterns of these genes (Figure 1B, HH21).

Further examination identified two more genes at this locus with right-sided expression: fatty acid elongase (*Elovl6*) and *Loc422694* (hereafter *cC4orf32*, ortholog of human *C4ORF32*) (Figures 1A–1C). This asymmetric pattern of expression was not exclusive to the DM. Asymmetries were present well prior to DM formation in the lateral mesoderm (precursor to the DM)

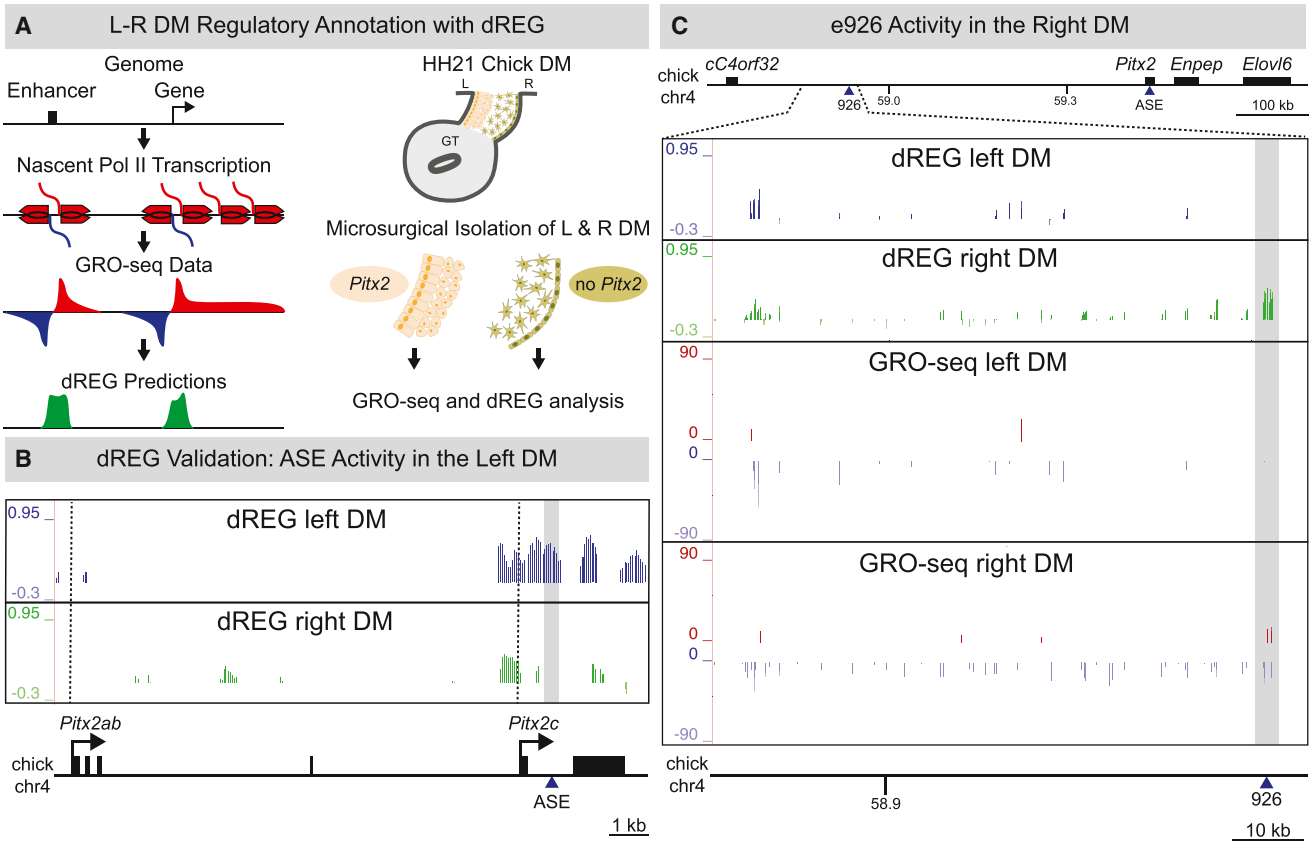

Figure 2. LR DM GRO-Seq/dREG Analyses

(A) (Left) GRO-seq and dREG. (Right) Libraries were prepared from HH21 LR DM samples.

(B) dREG peaks corresponding to ASE are left specific (gray box). Dashed vertical lines mark Pitx2ab and Pitx2c TSSs.

(C) dREG peaks overlapping e926 are right specific (gray box) in contrast to left-specific e926 transgenic reporter activity. GRO-seq detects asymmetric transcription from the minus strand at the proximal gene desert in the right DM. See also Figures S2 and S3.

(Figure 1B, HH17) and in the heart, where *Pitx2* also plays an essential role (Figure 1B, HH12) (Franco and Campione, 2003). The importance of the *Pitx2* locus during embryogenesis is underscored by strict conservation of its gene content, order, and orientation from humans to frogs, suggesting that functional and regulatory constraints maintain such synteny (Kikuta et al., 2007; Nobrega et al., 2003; Figure 1C).

Identification of Asymmetric Regulatory Element e926 at the *Pitx2* Locus

Asymmetric *Pitx2c* expression requires the ASE enhancer element located in the last intron of *Pitx2* (Shiratori et al., 2006). ASE functional activity is highly conserved, and homologous ASE sequences from fish, frog, chicken, mouse, and human drive left-specific reporter gene activity in mice (Shiratori et al., 2001, 2006). We hypothesized that additional elements exist in the gene desert that govern robust LR expression of neighboring genes. Such deserts, devoid of protein-coding genes, commonly contain regulatory elements (REs) that determine spatiotemporal expression of nearby genes.

We searched the Vista Enhancer Database (Visel et al., 2007) in the area of the gene desert and identified hs926, a human-derived sequence highly conserved among human, mouse, and chicken (Figure 1C). Element 926 (e926, 1,614 bp) showed reproducible enhancer-like activity in the midgut of whole-mount E11.5 transgenic reporter embryos (Figure 1D, n = 4/7), and it drove robust lacZ reporter activity specifically in the left DM of the midgut and duodenum (for Figure 1D and Figure S1, n = 3/3; transgenic embryos kindly provided by the Vista Enhancer group). Interestingly, right-specific e926 enhancer activity was noted in the heart (Figure S1, n = 2/3). Thus, e926 functions as an operational enhancer in transgenesis assays, and it responds both to the left and right regulatory environments in the DM and other asymmetric organs.

Right-Specific Regulatory Activity of e926 In Vivo

Since enhancers may act differently in *trans* as single elements or in the *cis* context of their endogenous loci (Marinić et al., 2013; Ruf et al., 2011; West et al., 2002), we sought to characterize e926 function in the DM. We used genome-wide global run-on sequencing (GRO-seq) of the left versus right DM (Figure 2A; Core et al., 2008). GRO-seq maps nascent transcription of engaged RNA polymerase II (Pol II) and collects strand-specific reads to identify regions of divergent transcription, a

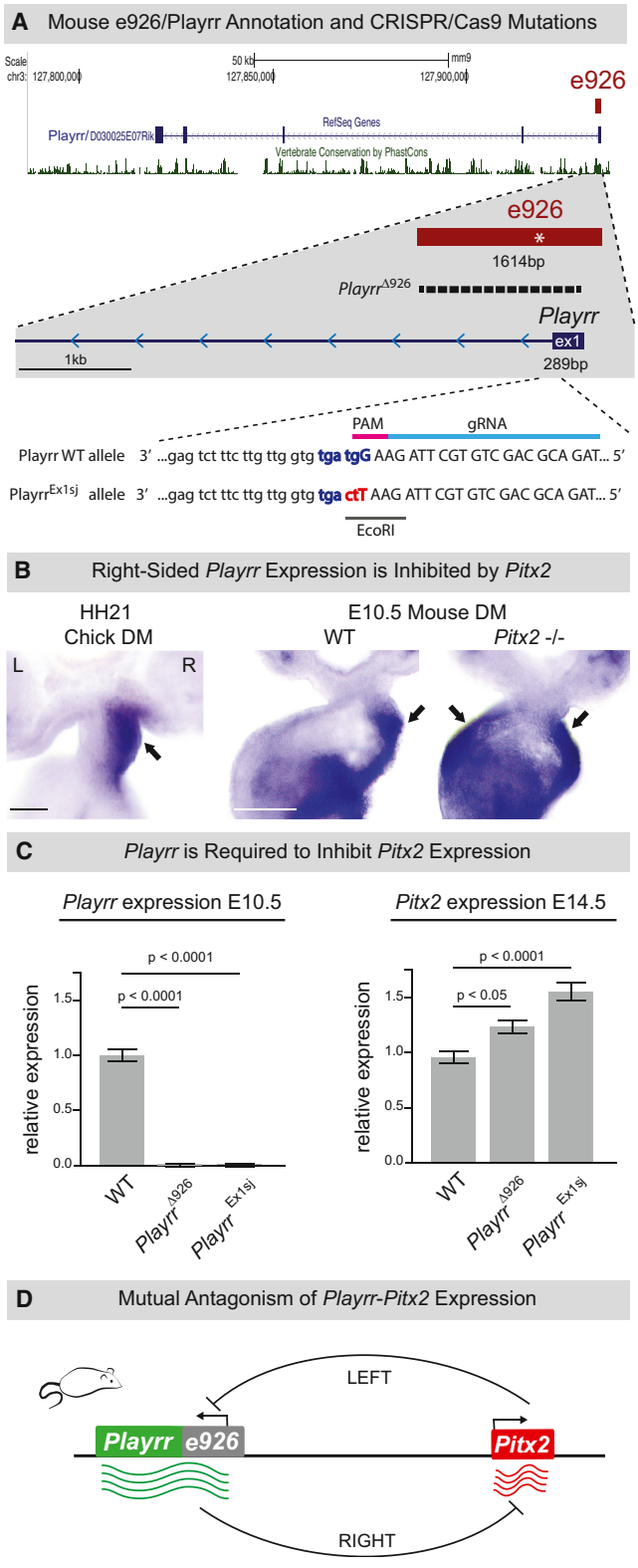

Figure 3. Identification of a Conserved lncRNA, *Playrr*, Asymmetrically Transcribed from e926

(A) Annotation of mouse lncRNA *Playrr* (D030025E07Rik). e926 contains the TSS and exon 1 of *Playrr* and a conserved *Pitx2*-binding motif (asterisk). CRISPR/Cas9 mutation of e926/*Playrr* (*Playrr*$^{\Delta 926}$, 1,420-bp dashed line; *Playrr*^{Ex1sj}, red and blue letters). Exon 1 (uppercase), intron 1 (lowercase), relative guide RNA (gRNA, light blue), and PAM motif (pink) were used to produce *Playrr*^{Ex1sj}.

(B) Whole-mount ISH shows right-specific *Playrr* in WT HH21 chicken and E10.5 mouse embryos versus bilateral *Playrr* expression in *Pitx2*-null mouse DM. Scale bars, 100 μm.

(C) The qRT-PCR expression in *Playrr*$^{\Delta 926}$ and *Playrr*^{Ex1sj} mutants (n = 3) relative to WT (n = 3) of *Playrr* (left) and *Pitx2* (right) at E10.5 or E14.5, respectively, is shown (error bars ± SEM).

(D) Mutual antagonism of *Playrr* and *Pitx2* expression is shown. See also Figures S1 and S4.

signature of active REs (Core et al., 2008, 2014; Melgar et al., 2011). We used discriminative regulatory element detection from GRO-seq (dREG), which recognizes the pattern of divergent transcription at active REs, to characterize the regulatory state of both nascent transcription and RE activation (Figure 2A, green; Danko et al., 2014).

Consistent with our microarray data, both GRO-seq and dREG analyses confirmed the binary LR gene expression from the *Pitx2* locus (Figure S2). For example, GRO-seq reads mapped to the asymmetric *Pitx2c* at the distal end of the desert only in the left DM samples, and dREG peaks at the ASE enhancer were also exclusively observed in the left samples (Figure 2B, gray box; Figure S3). In contrast, GRO-seq and dREG detected extensive transcription of the proximal desert preferentially in the right DM (Figure 2C; Figure S2), with dREG peaks at the e926 enhancer (Figure 2C, gray box). This confirms e926 as an asymmetrically responsive *cis*-RE, but contrasts starkly with the transgenesis assay, which suggested a left-specific activity (Figure 1D).

Identification of a Conserved lncRNA, Playrr, Transcribed from e926 on the Right Side

An alternative explanation for the discrepancy in asymmetric activity of e926 is that this RE functions not as an enhancer, but as a gene promoter in the right DM. However, no genes are annotated within this region of the chicken gene desert. Interestingly, GRO-seq reads extended a considerable distance from e926, suggesting a potential gene transcribed from the minus strand toward *cC4orf32* (Figure 2C, GRO-seq right DM). Supporting this hypothesis, the syntenic region of the mouse genome is annotated with D030025E07Rik, a lncRNA with a transcriptional start site (TSS) contained within e926 that also is transcribed from the minus strand of mouse chromosome 3 (Figure 3A). We generated clones and RNA probes from D030025E07Rik and chicken ESTs from this transcribed region. In both species, expression of this lncRNA was restricted to the right side of the DM consistent with the GRO-seq data (Figure 3B), suggesting a conserved lncRNA is expressed on the right side, opposite to *Pitx2*. We refer to this lncRNA as *Playrr* (*Pitx2* locus-asymmetric regulated RNA).

Mutual Antagonism of *Pitx2* and *Playrr* Expression In Vivo

We found conserved *Pitx2*-binding sites within e926, suggesting that *Pitx2* regulates *Playrr* expression (Figure S1B). To test this in vivo, we examined *Playrr* expression in the DM of E10.5 *Pitx2*−/− mouse embryos. In the absence of *Pitx2*, we found

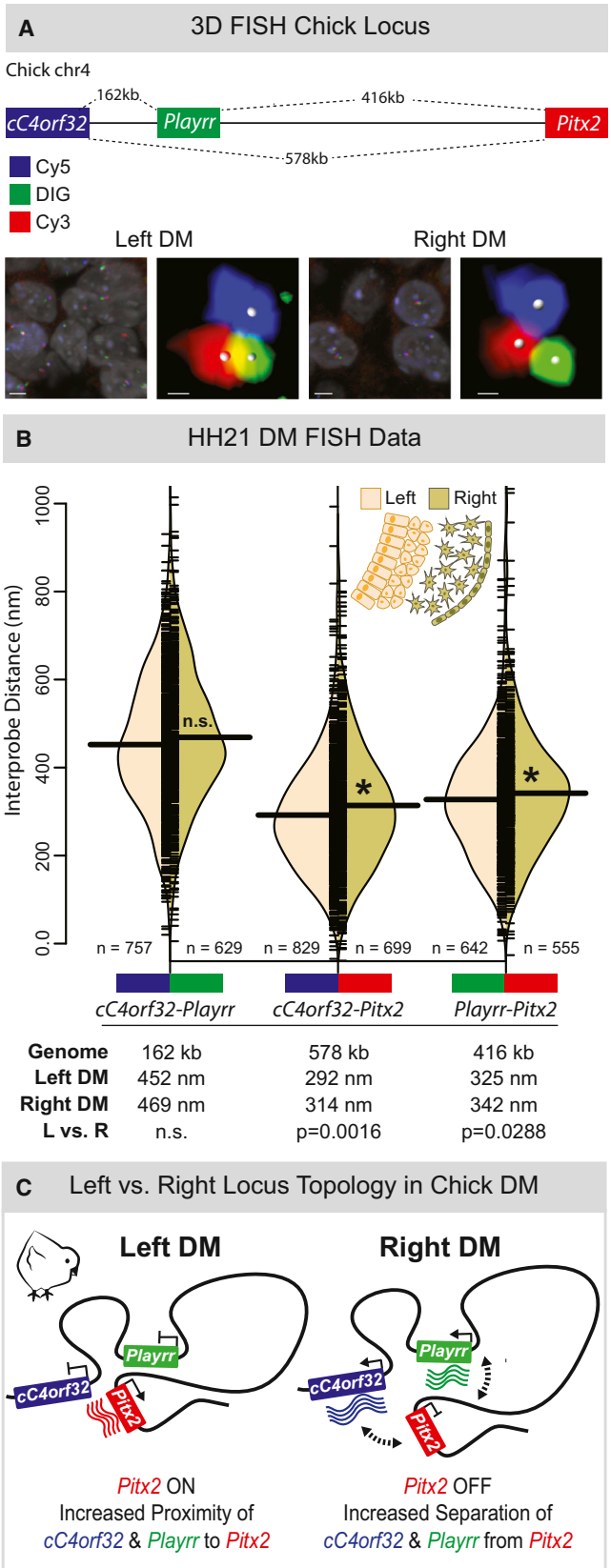

Figure 4. Asymmetric Chromatin Interactions of the *Pitx2* Locus in the Chicken LR DM

(A) Linear genomic distances in the chicken separating *cC4orf32*, *Playrr*, and *Pitx2* marked with Cy5-, DIG-, and Cy3-labeled DNA probes, respectively. FISH-labeled nuclei and individual loci in the left and right DM are shown. Scale bars, 2 μm and 300 nm for nuclei and individual loci, respectively.

(B) Split beanplots of interprobe distances for each probe pair (WT, HH21). Individual measurements are plotted as short horizontal ticks, and the density trace and mean are plotted as the filled curve and large horizontal bar, respectively. Table summary of distances separating each probe pair in the linear genome or nucleus is given.

(C) Model of *Pitx2* locus organization and gene expression in the chicken DM is shown. See also Figure S4.

that *Playrr* was expressed bilaterally in the DM (Figure 3B). Using qRT-PCR, we confirmed upregulation of *Playrr* expression in whole *Pitx2*−/− embryos, while other locus genes were unaffected. This indicates that, in the left DM, *Pitx2* specifically represses *Playrr* expression (Figure S4C).

To uncouple e926 and *Playrr* function during *Pitx2* locus expression (Figure 3A), we used CRISPR/Cas9 genome editing. We first targeted the proximal and distal ends of e926, simultaneously, deleting e926 and disrupting *Playrr* transcription ($Playrr^{\Delta 926}$). Second, to disrupt *Playrr* while leaving e926 intact, we mutated 3 bp of the U1 small nuclear ribonucleoprotein particle (snRNP) recognition sequence (ggtagt) at the 3′ end of *Playrr* exon 1 ($Playrr^{Ex1sj}$) (Figure 3A), leading to intron retention and exosomal degradation (Almada et al., 2013). Loss of detectable *Playrr* RNA was confirmed by qRT-PCR in both $Playrr^{\Delta 926}$ and $Playrr^{Ex1sj}$ E10.5 embryos (Figure 3C). Importantly, significant upregulation of *Pitx2* was found in E14.5 organ primordia of both $Playrr^{\Delta 926}$ and $Playrr^{Ex1sj}$ embryos compared to WT littermates (Figure 3C, E14.5). These data demonstrate mutual antagonism between *Pitx2* and *Playrr* expression and establish that function of the lncRNA *Playrr* is required to modulate *Pitx2* expression levels (Figure 3D).

Asymmetric Chromatin Looping of the *Pitx2* Locus in the Chicken DM

The contralateral expression of *Pitx2* and *Playrr*, their mutual antagonism, and evolutionary conservation of their arrangement on the chromosome suggest they may be regulated by chromosome structure. To address this, we employed multi-color 3D DNA FISH on chicken DM sections (3D tissue FISH). We used DNA probes (15–20 kb) to label *cC4orf32* (Cy5, blue) at the proximal gene desert, *Playrr* (DIG, green) within the desert, and *Pitx2* (Cy3, red) at the distal desert (Figure 4A). Quantified interprobe distances (i.e., *cC4orf32-Playrr*, *cC4orf32-Pitx2*, and *Playrr-Pitx2*) were used to determine the position of these loci in 3D space relative to each other and to the intervening desert.

Within the genome, *cC4orf32* and *Playrr* are nearest each other, separated by 162 kb (compare to 578 kb between *cC4orf32* and *Pitx2* and 416 kb between *Playrr* and *Pitx2* [Figure 4A]). However, our FISH revealed that, within DM nuclei, both *cC4orf32* and *Playrr* were significantly closer to *Pitx2* than to each other (Figure 4B). This striking interaction brings far-separated genes (416 and 578 kb) into closer spatial proximity than genes separated by just 160 kb. Our data,

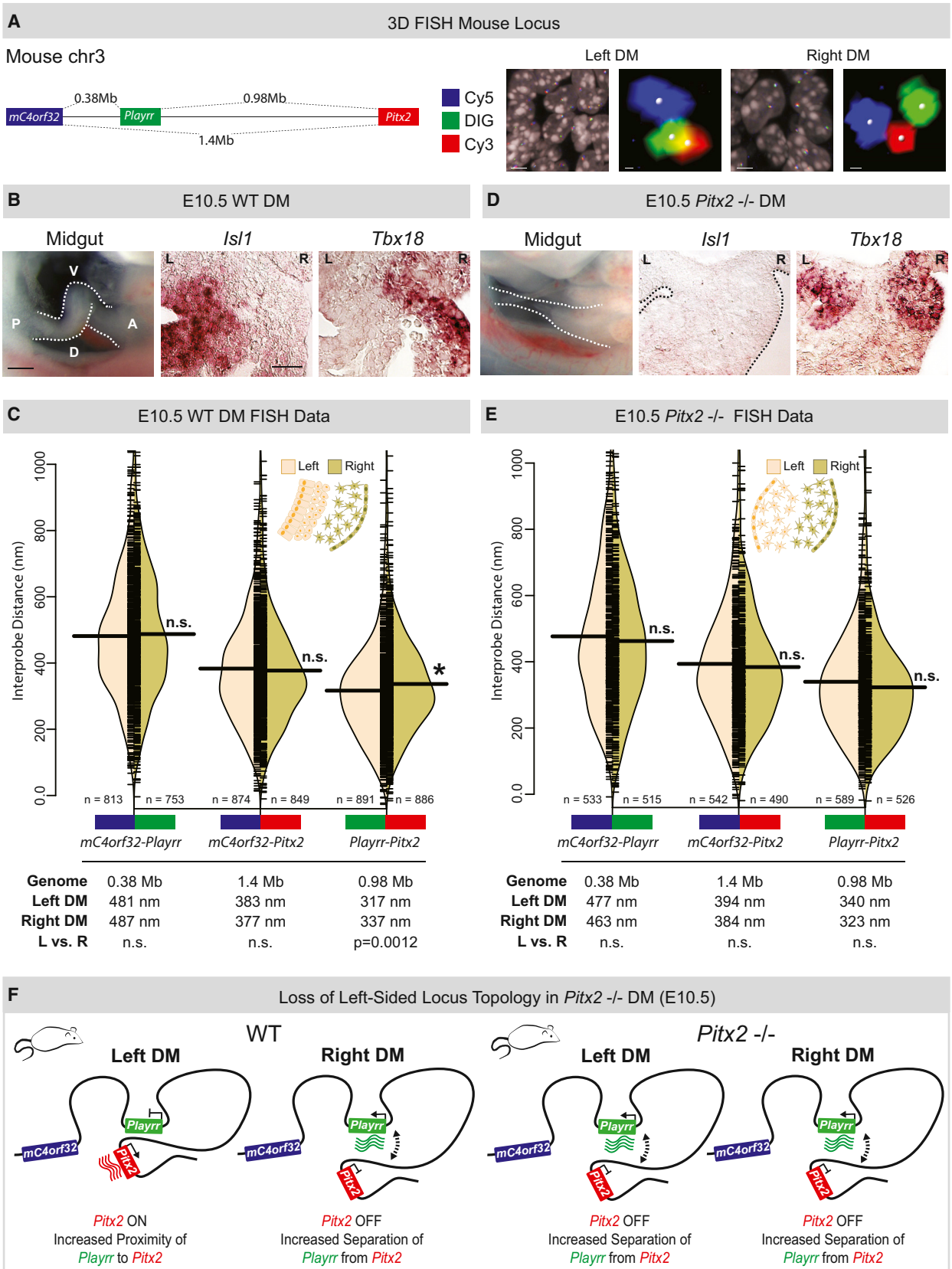

(legend on next page)

therefore, establish that long-range looping of the *Pitx2* locus positions the proximal and distal ends of the gene desert in close 3D proximity.

The global architecture of the Pitx2 locus is similarly organized in the left and right DM (Figures 4B and 4C). Importantly, however, we identified subtle but statistically significant LR differences in interprobe distances for both *cC4orf32-Pitx2* and *Playrr-Pitx2*, demonstrating closer proximity of both *cC4orf32* and *Playrr* to *Pitx2* in the left DM compared to the right (Figure 4B; Figure S4A). LR differences in these distances were reproducible across five replicate experiments (Figure S4). Hence, mirroring the asymmetric gene expression and cellular architecture in the DM, proximity of *cC4orf32*, *Playrr*, and *Pitx2* DNA in nuclei of the left DM is associated with preferential transcription of *Pitx2*. Conversely, in the right DM, where *cC4orf32* and *Playrr* are expressed, they are farther separated from *Pitx2* (Figure 4C). Thus, LR differences in 3D looping of the *Pitx2* locus are characterized by subtle local shifts, rather than global differences, in the positioning of genes within a constant overall locus topology.

Spatial Proximity of *Playrr* and *Pitx2* Is a Conserved Feature of Locus Topology

To address the degree to which asymmetric nuclear architecture of the chicken *Pitx2* locus is conserved, we used the same FISH-labeling scheme on mouse DM sections and analyzed pairwise interprobe distances for 5730508B09Rik (*mC4orf32*, the mouse ortholog of *C4ORF32*, Cy5, blue) in the proximal desert, *Playrr* (DIG, green) within the desert, and *Pitx2* (Cy3, red) at the distal desert (Figure 5A). In the mouse genome, the linear genomic distance separating the FISH probe pairs *mC4orf32-Playrr*, *mC4orf32-Pitx2*, and *Playrr-Pitx2* was 380 kb, 1.36 Mb, and 980 kb, respectively (Figure 5C).

Consistent with the chicken DM, long-range looping across the mouse gene desert positions *mC4orf32* and *Playrr* in significantly closer proximity to *Pitx2* than to each other (Figure 5C). Remarkably, though mouse *Playrr* is located nearly twice the genomic distance proximal to *Pitx2* compared to chicken, the interprobe distance measured for *Playrr-Pitx2* was nearly identical to that measured in chicken (Figures 4B and 5C). Moreover, *Playrr-Pitx2* spatial proximity in the left versus the right DM was maintained in the mouse, further highlighting our observation that proximity of *Playrr* and *Pitx2* on the left is associated with preferential *Pitx2* transcription (Figure 5C). In contrast, the position of *mC4orf32* relative to both *Playrr* and *Pitx2* was farther than observed in chicken and not different in nuclei on the left versus right (Figures 5C and 5F), a finding accompanied by the bilateral expression of *mC4orf32* in mouse DM (Figure S6A). Thus, small differences in the positions of genes relative to each other have direct consequences on their asymmetric expression. Collectively, LR asymmetry in nuclear proximity of *Playrr* to *Pitx2* is a conserved feature of *Pitx2* locus topology.

Altered LR Patterning Disrupts Asymmetric *Pitx2* Locus Topology

In mice lacking *Pitx2*, the left DM fails to condense, all LR DM asymmetry is lost, and stereotypical gut looping is randomized (a double-right phenotype) (Figure 5D; Davis et al., 2008; Kurpios et al., 2008). *Pitx2*-null embryos lose left-specific expression of *Pitx2* target genes such as *Islet1* (Figure 5D), and they show bilateral expression of right-sided genes, such as *Tbx18* (Figure 5D) and *Playrr* (Figure 3C). To investigate whether the subtle LR differences of locus topology are similarly affected, we performed 3D tissue FISH on *Pitx2*-null mouse DM. Importantly, we found that global locus topology was maintained, while the proximity of *Playrr* and *Pitx2* in the left WT DM was lost in *Pitx2*-null embryos (Figure 5E). Hence, in the absence of *Pitx2*, *Playrr* and *Pitx2* are significantly farther apart in the left DM compared to the WT left DM, and indistinguishable from WT interprobe distances in the right DM (Figures 5C and 5E; Figure S4). Thus, a double-right phenotype of the *Pitx2*-null DM is accompanied by isomerized nuclear architecture at the *Pitx2* locus (Figure 5F). These data indicate that *Pitx2* is required for asymmetric positioning of individual loci within the overall locus topology (Figure 5F).

Analysis of *Playrr-Pitx2* Chromatin Interactions in mESCs

The chromatin regulatory landscape within mouse embryonic stem cells (mESCs) has been extensively characterized. Reanalyses of existing Pol II chromatin immunoprecipitation sequencing (ChIP-seq) data (Kagey et al., 2010) demonstrate that mESCs express the LR asymmetric *Pitx2c* isoform (Figure 6A), while *mC4orf32* is expressed at low levels and *Enpep* and *Playrr* are undetectable. *Pitx2c* expression in these cells is accompanied by activation of the asymmetric ASE enhancer (Figure S7; Creyghton et al., 2010). We therefore leveraged available chromatin interaction datasets to analyze locus topology associated with *Pitx2c* expression in mESCs (Shen et al., 2012; Dowen et al., 2014) to model the left-specific transcriptional and regulatory profile of the locus.

We defined looping interactions using HiC, a genome-wide variation of 3C, and chromatin interaction analysis by paired-end tag sequencing (ChIA-PET) (de Wit and de Laat, 2012). Both HiC and Smc1 ChIA-PET demonstrated enriched long-range interactions at the *Pitx2* locus compared to flanking regions, data consistent with a topologically associating domain (TAD). Importantly, these data suggest the division of the TAD

Figure 5. Spatial Proximity of *Playrr-Pitx2* Chromatin Interactions Are Dependent on Pitx2

(A) Linear genomic distances in the mouse separating *mC4orf32*, *Playrr*, and *Pitx2* marked with Cy5-, DIG-, and Cy3-labeled DNA probes, respectively. FISH-labeled nuclei and individual loci in the left and right DM are shown. Scale bars, 2 μm and 300 nm for nuclei and individual loci, respectively.

(B) Chiral looping of the WT midgut is accompanied by left-specific *Isl1* and right-specific *Tbx18*. A, anterior; P, posterior; D, dorsal; V, ventral. Scale bars, 250 and 25 μm for whole mount and section, respectively.

(C) Split beanplots (WT E10.5). Table summary of distances separating each probe pair in the linear genome or nucleus is given.

(D) Altered midgut looping and right-isomerized DM in *Pitx2*-null embryos is evidenced by loss of left-specific *Isl1* and bilateral *Tbx18* expression.

(E) Split bean plots are shown (Pitx2-null E10.5).

(F) Model of *Pitx2* locus organization and gene expression in the mouse DM is shown. See also Figure S4.

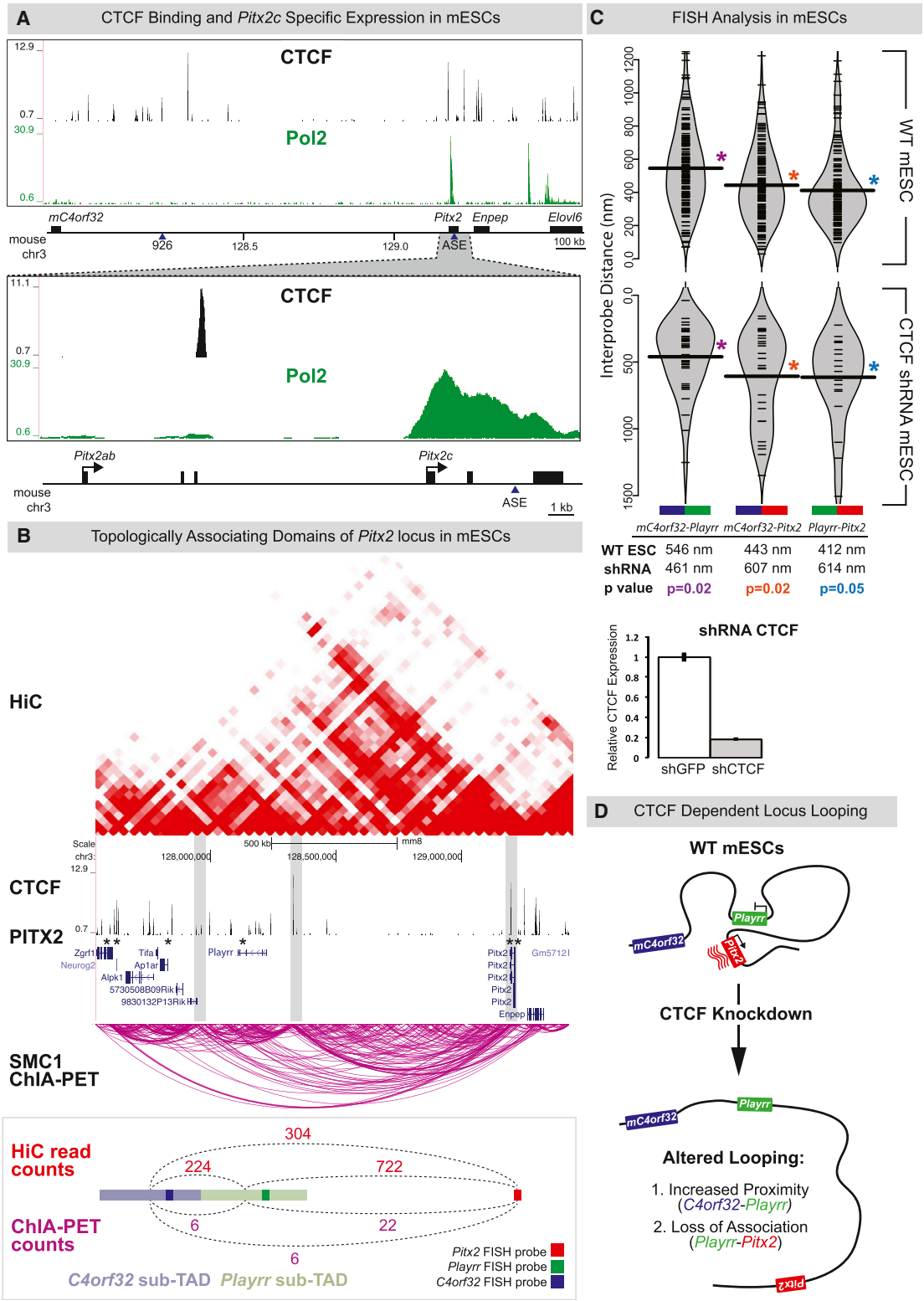

Figure 6. *Playrr-Pitx2* Chromatin Interactions in mESCs Are Dependent on CTCF

(A) (Top) CTCF binding at the *Pitx2* locus (CTCF ChIP-seq). (Bottom) The mESCs preferentially express the asymmetric *Pitx2c* isoform (Pol II ChIP-seq).

(B) A topologically associating domain (TAD) spans the *Pitx2* locus (HiC, red; Smc1 ChIA-PET, magenta). Vertical gray bars highlight boundaries between sub-TADs. CTCF-binding sites (ChIP-seq) at both *Pitx2* and *Playrr* are associated with Pitx2 binding (Pitx2-FLAG ChIP-seq, asterisks). Quantification of HiC (red) and

(legend continued on next page)

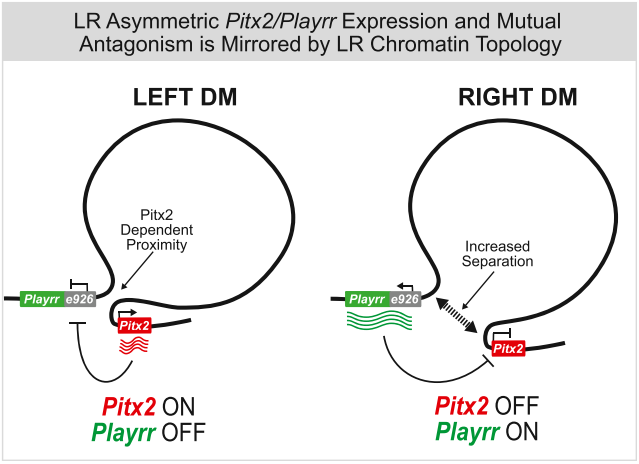

Figure 7. Summary of *Pitx2* Locus Asymmetric Expression and Chromatin Topology

In chicken and mouse, left-specific *Pitx2* expression and right-sided expression of flanking genes at the *Pitx2* locus, including the conserved lncRNA *Playrr*, is accompanied by Pitx2-dependent asymmetric chromatin topology in the DM. In vivo, *Pitx2* expression and *Playrr* expression are mutually antagonistic.

into sub-TADs that correlate with the position of our DNA FISH probes (Figure 6B).

To determine if proximity of *Playrr* to *Pitx2* versus *mC4orf32* accompanies *Pitx2c* expression in mESCs as observed in vivo, we quantified HiC and ChIA-PET reads linking the *mC4orf32* and *Playrr* sub-TADs with each other and to *Pitx2* (Figure 6B, bottom). Significantly, although *Playrr* was 2.5 times farther from *Pitx2* than from *mC4orf32*, the *Playrr* sub-TAD interaction with *Pitx2* was nearly four times greater than with the adjacent *mC4orf32* sub-TAD (Figure 6B, bottom).

Finally, we performed FISH on WT mESCs. We found that the 3D organization of the *Pitx2* locus in mESCs is nearly identical to mouse DM, with *Playrr-Pitx2* closest and *mC4orf32-Playrr* farthest separated (Figure 6C, top). Thus, genome-wide molecular analysis and direct visualization together confirm the preferential association of *Playrr* with *Pitx2* that accompanies asymmetric *Pitx2* expression.

CTCF Is Essential for Maintaining the Long-Range *Playrr-Pitx2* Interaction

CCCTC-binding factor, CTCF, is a sequence-specific scaffold protein that, by interaction with proteins such as Cohesin and Mediator, directs long-range looping to shape cell-type-specific chromatin architecture (Splinter et al., 2006; Phillips-Cremins et al., 2013).

CTCF ChIP-seq data from mESCs identified CTCF-binding peaks in the proximal gene desert near *mC4orf32* and *Playrr* (Figure 6B; Kagey et al., 2010). Both Smc1 ChIA-PET and CTCF ChIP-seq highlighted that the *Playrr-Pitx2* interaction is mediated by CTCF sites within the *Pitx2* gene and upstream of e926/*Playrr* (Figures 6A and 6B). Significantly, Pitx2-FLAG ChIP-seq in vivo established that the CTCF-binding sites at both *Pitx2* and *Playrr* also may be associated with Pitx2 binding (Figure 6B; Tao et al., 2014).

We knocked down CTCF in mESCs (Figure 6C), which abrogated long-range looping across the gene desert and disrupted global chromatin organization of the locus (Figures 6C and 6D) compared to WT mESCs. Significantly, CTCF knockdown also decreased the distance separating *mC4orf32-Playrr* (mean separation of 546 versus 461 nm in WT versus CTCF knockdown) and abolished the close proximity of *Playrr* to *Pitx2* (mean separation of 412 versus 614 nm in WT versus CTCF knockdown). This demonstrates a requirement for CTCF during long-range chromatin looping at the *Pitx2* locus, a prerequisite for *Pitx2*-dependent regulation of laterality (Figure 6D).

DISCUSSION

Pitx2 expression governs transcriptional programs that determine asymmetric organ morphology. In the DM, left-sided *Pitx2* regulates molecular and cellular asymmetry required to loop and vascularize the gut (Davis et al., 2008; Kurpios et al., 2008; Welsh et al., 2013; Mahadevan et al., 2014). We now show this binary LR tissue organization is mirrored by transcriptional output and chromatin architecture at the *Pix2* locus in the left versus right DM (Figure 7).

Our 3D tissue FISH analyses characterized how the conserved genomic interval harboring *Pitx2* is organized in 3D space to effect asymmetric gene expression and LR patterning. The topology of the *Pitx2* locus, as measured optically, demonstrates both global and local organizational principles consistent with HiC and ChIA-PET data from mESCs, an in vitro model for left-specific *Pitx2* locus transcription. In chicken and mouse, we established that long-range chromatin looping across a large gene desert is a conserved and constitutive feature of *Pitx2* locus organization, dependent on CTCF. Within this constitutive topology, we showed that *Playrr-Pitx2* are in closer proximity in the left DM where *Pitx2* is preferentially expressed, but positioned farther apart in the right DM where *Playrr* is expressed and *Pitx2* is not (Figure 7). While LR differences in interprobe distances were notably small, they were reproducible across biological replicates, models, and organisms. Moreover, the mean *Playrr-Pitx2* interprobe distance in the left DM of *Pitx2*-null mice was similar to that on the right side of both Pitx2−/− and WT mice, showing these LR differences are *Pitx2* dependent. Our FISH analysis only marked the relative position of asymmetrically expressed genes in the left or right DM, and it is likely that the subtle LR proximity differences were actually

Smc1 ChIA-PET (magenta) interactions between the genomic interval containing the *Pitx2* FISH probe and the *Playrr* sub-TAD (light green) compared to the *mC4orf32* sub-TAD (light blue) is shown.

(C) FISH analysis of *Pitx2* locus topology in WT (top) or shRNA-mediated CTCF knockdown mESCs (bottom, y axis has been inverted). Table gives summary of distances separating each probe pair in the nucleus. CTCF expression via qRT-PCR in control versus CTCF knockdown mESCs is shown (error bars ± SEM).

(D) Summary of *Pitx2* locus topology in mESCs is shown. See also Figure S7.

secondary to interactions between promoters and sequences that we have not labeled. Indeed, both HiC data and Smc1 ChIA-PET in mESCs demonstrated that the preferential interaction between *Playrr* and *Pitx2* likely involves looping between CTCF sites near e926/*Playrr* and within the *Pitx2* gene (Figure 6B).

TAD boundaries are enriched in CTCF binding (Dixon et al., 2012; Nora et al., 2013; Phillips-Cremins et al., 2013). TAD structure also correlates with blocks of genomic synteny, and thus changes in their structure are likely evolutionarily constrained (Dixon et al., 2012; Nora et al., 2013). We showed that CTCF is required for maintenance of the megabase-scale topology of the *Pitx2* locus, characterized via 3D FISH. However, different gene expression patterns in chicken versus mouse are consistent with significant differences in positioning of the proximal, but not distal, gene desert. Interestingly, in mESCs, binding of CTCF downstream of exon 3 of the bilaterally expressed *Pitx2a* overlapped a conserved CTCF recognition sequence in chicken (Figure 6B), while CTCF-binding sites proximally in the vicinity of *C4orf32* appeared to lack strict conservation. Interestingly, the gene desert is conserved in zebrafish, but they lack a *C4ORF32* ortholog, suggesting evolutionary divergence of the proximal gene desert (Figure S6C; Volkmann et al., 2011). Furthermore, while *Elovl6* is present, the zebrafish *Pitx2* locus lacks an *Enpep* ortholog, and although both chick and mouse loci possess *Enpep*, this gene is not expressed in the mouse DM compared to its right-sided expression in chicken. Hence, despite changes in gene content and regulatory refinement at the *Pitx2* locus during evolution, control over *Pitx2* spatial expression has been maintained. Consistent with this hypothesis, the HiC interaction map of mESC suggests that *Pitx2* and *Enpep* are partitioned into separate regulatory domains (Figure 6B). Thus, while the *Pitx2* locus in chicken and mouse exhibits conserved architecture, species-specific differences have consequences on spatial gene expression and may result from the acquisition or turnover of CTCF binding.

Our study demonstrates the utility of combining genome-wide analyses in vivo to characterize nascent transcription and RE activity within a single sample. An unanticipated finding from this approach was the identification of *Playrr* as an asymmetrically expressed lncRNA derived from the conserved e926 RE. Rather than matching the left-specific enhancer activity of e926 observed in transgenic embryos, we showed that *Playrr* is exclusively expressed in the right DM. Thus, dREG mapping of active REs in situ highlights one caveat of testing putative *cis*-regulatory sequences in *trans*, isolated from their endogenous context (Marinić et al., 2013).

A coherent understanding of the biological roles of lncRNAs is still lacking, although one of transcriptional regulation is an emerging theme (Rinn and Chang, 2012; Vance and Ponting, 2014). Recent analysis of the *trans*-acting lncRNA *Fendrr*, which interacts with the polycomb repressive complex 2 (PRC2), establishes a role for lncRNAs in the regulation of *Pitx2* expression (Grote et al., 2013). Although the impact on LR patterning was not addressed, mutation of *Fendrr* causes loss of *Pitx2* silencing and altered differentiation of the lateral mesoderm (Grote et al., 2013; Grote and Herrmann, 2013). We now show that *Playrr*, an lncRNA asymmetrically expressed from the *Pitx2* locus itself, also acts to modulate *Pitx2* expression. Interestingly, expression of *Fendrr* is restricted to gastrulation stages of development, while *Playrr* is expressed later during organogenesis. Significantly, evidence for auto-regulation of asymmetric gene expression by *Pitx2* has been documented during heart and limb development (Shiratori et al., 2006, 2014). The contralateral expression and mutual antagonism of *Playrr* and *Pitx2* expressed from the same locus suggest e926/*Playrr* is an integrated regulatory module that provides such auto-regulation. Since the function of many lncRNAs likely depends on structural conformations permissive of DNA, RNA, or protein interactions (Rinn and Chang, 2012; Nitsche et al., 2015; Johnsson et al., 2014), further characterization of our $Playrr^{Ex1sj}$ mutant provides a unique means to address the specific mechanisms through which *Playrr* influences *Pitx2* locus output. Finally, *Pitx2* expression is required in dynamic spatial patterns during development, where individual isoforms play dose-dependent roles in diverse tissues (Liu et al., 2001; Waite et al., 2013). Notably, midgut looping requires high levels of *Pitx2c* and is sensitive to bilateral misexpression of *Pitx2c* (Liu et al., 2001). Thus reciprocal interactions between *Pitx2* and e926/*Playrr* likely provide an organ-intrinsic mechanism for tight Pitx2 dosing.

Mutations of human *PITX2* result in a spectrum of ARS-associated birth defects and predispose individuals to cardiac fibrillation and arrhythmia (Semina et al., 1996; Tao et al., 2014; Wang et al., 2014). Conservation of the gene desert at the locus and the number of noncoding mutations identified in human ARS patients likely reflects the regulatory complexity required to fine-tune *Pitx2* expression. Knowledge of the mechanisms that direct *Pitx2* spatiotemporal expression is as critical as defining its downstream targets. Our work begins to shed light on the *cis*-regulatory mechanisms and etiology of ARS and *Pitx2*-associated AF, offering unprecedented potential to develop mouse models of these important human diseases.

EXPERIMENTAL PROCEDURES

Animals

WT and *Pitx2* mutant embryos, $Pitx2^{hd}$ allele (Lu et al., 1999), were collected from timed matings, with the morning of the plug defined as E0.5. Fertile eggs (White Leghorn) obtained from the Cornell Poultry Farm were incubated at 38°C and staged (Hamburger and Hamilton, 1992). Experiments adhered to guidelines of the Institutional Animal Care and Use Committee of Cornell University, under the Animal Welfare Assurance on file with the Office of Laboratory Animal Welfare.

Laser Capture Microdissection and Microarray

Detailed methods and full microarray results are in preparation to be published elsewhere. Briefly, cryosections of unfixed/flash-frozen WT HH21 chicken DM were arrayed on membrane slides (Leica, 11505189). The asymmetric morphology of the left and right DM was used to discriminate and capture separately each compartment. Three separate biological experiments of four cell compartments were performed, giving 12 microarray samples (biological triplicate). RNA was isolated using the PicoPure RNA Isolation kit (Arcturus, KIT0202), and cDNA was prepared using the WT-Ovation Pico kit (NuGEN). Affymetrix cRNA target-labeling reactions were carried out per the manufacturer instructions, and GCOS output files were loaded into GeneSpringGX 7.3 or GeneSpring 13 software packages (Agilent Technologies) for expression analyses.

RNA In Situ Hybridization

The 250-μm-thick embryo slices for whole-mount RNA in situ hybridization (ISH) were collected with a McIlwain tissue chopper (Campden Instruments),

fixed in 4% paraformaldehyde (PFA)/PBS overnight, dehydrated, and stored in 100% methanol prior to processing. Whole-mount ISH followed standard protocols as previously described (Welsh et al., 2013).

Statistical Analysis

Measurement data were analyzed with R and Mann-Whitney-Wilcoxon test was used to compare interprobe distances in FISH experiments; data were plotted with the beanplot package in R (Kampstra 2008). Boxplots of FISH data in Figure S4 were generated using JMP Pro 11. Student's t test was used for comparison of qRT-PCR data; error bars show ± SEM.

LR GRO-Seq and dREG Analysis

Whole embryos (n = 250) were chopped into 250-μm transverse slices using a McIlwain tissue chopper, followed by manual microdissection of the left and right DM. Collected tissues were pooled, snap frozen in liquid nitrogen, and stored at −80°C until processing (Core et al., 2008). We also performed GRO-seq on whole embryos (HH21, n = 2), on embryonic heads (HH12, n = 250), and on the left and right hemisected embryos (HH12, n = 250). The dREG analysis of GRO-seq datasets is available via GitHub (https://github.com/Danko-Lab/dREG).

Cloning, Plasmids, and Oligonucleotides

Full-length cDNAs and RNA probes were cloned using TA cloning (Invitrogen) and oligo-dT primed cDNA reverse transcription (Superscript III, Invitrogen) from RNA pooled from HH19 and HH21 whole chicken or from E8.5–E18.5 whole mouse embryos. Cloned DNA was sequence verified.

CRISPR/Cas9 Targeting of e926/Playrr

The following guide RNAs were designed (http://crispr.mit.edu/; Hsu et al., 2013) and cloned into BbsI cut pX330: Playrr, TAGACGCAGCTGTGCTTAGAAGG; e926 proximal, GTGGCGGACTCATGTTAAAAAGG; e926 distal, GTGATTCCCACCACGCTTTGAGG. For Playrr targeting, the 156-bp single-stranded oligodeoxynucleotide (ssODN) used as a repair template carries a 3-bp change to disrupt the 5′ splice site of Playrr exon 1 and introduce an EcoRI restriction site for genotyping (see Figure 3). The single-guide RNA (sgRNA) was in vitro transcribed (Ambion MEGAshortscriptT7 kit) from a PCR-generated template and purified (Ambion MEGAclear kit). Each sgRNA (50 ng/μl), ssODN (10 ng/μl), and Cas9 mRNA (100 ng/μl) were injected into F1 hybrid (C57BL/6J × FvB/N) one-cell embryos. Injected embryos were cultured to the two-cell stage prior to transfer to recipient females. Two independent lines were established and analyzed for each mutation.

qRT-PCR

Embryonic tissue was isolated in cold PBS, stored in RNAlater until extraction (QIAGEN RNeasy miniprep kit). For cultured cells, RNA was extracted using 4–6 × 10^6 cells. RNA (2 μg) was reverse transcribed using the ABI high-capacity cDNA archive kit and diluted to 20 ng/μl. The following TaqMan gene expression assays were used for relative quantification (ABI7500): Actb, Mm00607939_s1; 5730508B09Rik (mC4orf32), Mm02375228_s1; D030025E07Rik (Playrr), Mm03937997_m1; CTCF, Mm00484027_m1; Enpep, Mm00468278_m1; GAPDH, Mm99999915_g1; Pitx2ab, Mm00660192_g1; Pitx2c, Mm00440826_m1; and pan-Pitx2, Mm01316994_m1.

FISH

The following bacterial artificial chromosomes (BACs) spanning either the chicken or mouse *Pitx2* locus were used: (chicken) CH261-95I8, CH261-66N5, CH261-187K8, CH261-34B16, CH261-110J5, CH261-91C24, and CH261-134M23; (mouse) RP23-306C6, RP23-328J13, RP23-225C17, RP24-98F15, RP23-266N9, RP23-106J9, RP23-150F9, RP24-156B21, RP24-100G2, and RP23-307L21. The genomic distances analyzed in this study are resolvable via interphase FISH (50–100 kb); to further maximize resolution, we designed probes to be less than 25 kb (Trask et al., 1991). Genomic intervals spanned by FISH probes and probe sizes were as follows: (chicken [galGal4]) cC4orf32 (23.8 kb), chr4:56,825,232-56,849,123; e926 (16 kb), chr4:56,989,104-57,005,206; and Pitx2 (17.5 kb), chr4:57,398,355-57,415,925; (mouse [mm10]) mC4orf32 (15.5 kb), chr3:127,846,052-127,861,644; e926 (16 kb), chr3:128,221,875-128,237,854; and Pitx2 (21 kb), chr3:129,199,824-129,221,272. Probes were labeled with dUTP-Cy3, -Cy5, or -DIG via nick translation of 1 μg DNA (Roche). Embryos were fixed overnight in 4% PFA and embedded in paraffin following standard protocol. Then 6-μm sections were collected on Superfrost plus slides, dried overnight at 37°C, baked at 60°C for 20 min, cooled, and then dewaxed in xylene with two washes for 10 min each, followed by two washes in 100% ethanol and one wash in 70% ethanol, 5 min each. Sections were treated for 5 min with 0.2 N NaOH in 70% ethanol to remove RNAs, washed twice in 70% ethanol, rehydrated, and washed 10 min in 0.1 M citrate buffer at 80°C. Sections were washed in water, equilibrated in 2× saline sodium citrate (SSC) for 5 min, denatured for 2.5 min at 79°C in 70% formamide/2× SSC, and hybridized overnight at 37°C with 50 ng probe, 10 μg species-specific Cot-1 DNA, 10 μg salmon sperm DNA, and 10 μg tRNA. Sections were washed with 2× SSC/50% formamide at 37°C, 2× SSC 37°C, 1× SSC at room temperature, for 15 min each. DIG-labeled probes were detected with AF488 anti-DIG-conjugated antibodies diluted 1:500 in 4× SSC/1% BSA. The mESCs were seeded onto coverslips, fixed in 4% PFA, and then permeabilized following published protocols (Kurz et al., 1996). Hybridization followed the same protocol with the exception that the citrate unmasking step was omitted.

Quantification of HiC and Smc1 ChIA-PET Interactions

Previously published HiC (Dixon et al., 2012; GEO: GSE35156) or ChIA-PET (Dowen et al., 2014; GEO: GSE57911) datasets were used to analyze chromatin interactions in mESCs linking the following genomic intervals (mm9): mC4orf32 sub-TAD, chr3:127279136–127674264; Playrr sub-TAD, chr3:127674265–128090964; and Pitx2 FISH probe, chr3:128902742–128924190. The boundaries of sub-TADs were defined based on CTCF peaks (Roadmap data). To quantify HiC interactions, the virtual 4C tool (http://promoter.bx.psu.edu/hi-c/) was used with rs47546564, rs31670515, and Pitx2 as anchor points for the mC4orf32 sub-TAD, Playrr sub-TAD, and Pitx2 FISH probe, respectively. Read counts across each genomic interval connected to an individual anchor point were summed. To quantify ChIA-PET interactions, we counted the number of PETs that had one end overlapping with Pitx2, mC4orf32, or mPlayrr FISH probes and the other end overlapping with individual sub-TADs by at least 1 bp. The count results were similar from two Smc1 ChIA-PET replicates; we therefore took the sum of the two and visualized the data in WashU genome browser.

Image Acquisition and Analysis for 3D FISH

Slides were imaged on a Zeiss 710 scanning laser microscope using a 63×/1.4 NA Plan-APOCHROMAT oil immersion objective and z series data were acquired using the optimal step size. Imaris image analysis software (Bitplane) was used to quantify interprobe distances. Following image filtering using baseline subtraction, FISH signals for each channel were defined using the built-in spot function, which segments the signal using a Gaussian filter-based background subtraction method and calculates the center of image mass of each segmented spot. The position of each spot object in (x, y, z) is equal to the value of the center of homogeneous mass of the object. Distance measurements between the center of mass for each signal was determined pairwise for each probe pair using the measurement point tool and verified by two independent investigators.

Lentiviral Production and Transduction

The 293FT cells were transfected with pLKO.1 lentiviral plasmids containing either small hairpin RNAs (shRNAs) targeting CTCF or GFP, along with the packaging plasmids pLP1, pLP2, and pLP/VSV-g, using Lipofectamine 2000. Viral media were collected and centrifuged at 3,000 rpm to pellet debris and then filtered through a 0.45-μm polyvinylidene fluoride (PVDF) filter and frozen until use. Virus-containing media were supplemented with additional fetal bovine serum (FBS), LIF, and 6 μg/ml polybrene, prior to use. WT ESCs, expanded on gamma-irradiated feeder cells, were trypsinized and plated for 30 min onto gelatin-free tissue culture plates to remove feeders prior to transduction. Following seeding ESCs at 2 × 10^6 cells/100-mm plate and incubation for 24 hr, media were exchanged with ES media supplemented with 6 μg/ml polybrene and plates were incubated for an additional 15 min at 37°C prior to exchanging media with virus-containing ES media. After transduction, media were exchanged for normal ESC media and cells were

incubated for an additional 24 hr prior to selection with 2 μg/ml puromycin. After 3 days of selection, ESCs were trypsinized and plated for FISH or collected for RNA.

ACCESSION NUMBERS

The microarray data have been deposited under accession number GEO: GSE71117.

SUPPLEMENTAL INFORMATION

Supplemental Information includes seven figures and can be found with this article online at http://dx.doi.org/10.1016/j.celrep.2015.08.075.

AUTHOR CONTRIBUTIONS

I.C.W. and N.A.K. designed the study. I.C.W. performed all the experiments with additional contributions from L.S.S. for FISH guidance and data analysis, H.K. for GRO-seq with guidance from J.T.L., C.G.D. for dREG analysis with guidance from H.K., F.L.C. for double-label RNA ISH (Figure 1B) and CRISPR/Cas9 deletion of e926 (Figures 3A and 3C), M.W. for RNA ISH, and M.Z. and J.F.M. for HiC and ChIA-PET computational analysis and quantifications (Figure 6B). I.C.W. and N.A.K. wrote the manuscript with input from all coauthors.

ACKNOWLEDGMENTS

We thank Dr. Len Pennacchio and Jennifer Akiyama (http://enhancer.lbl.gov) for providing archived embryos; Drs. Victor Corces, Stephen Dalton, and Yuhua Sun for shRNA constructs; David Gludish for technical expertise on shRNA and for microarray analyses; and Dr. John Schimenti for discussions and stocks of mESCs. Jason Crossley, Michelle Miller, and Sriharsha Ponna provided technical assistance. We are grateful to Aravind Sivakumar, Aparna Mahadevan, and other members of the N.A.K. lab for feedback on the manuscript. We thank Cornell Biotechnology Resource Center Imaging Facility and Carol Bayles for assistance with microscopy (NIH 1S10RR025502-01) and Rob Munroe and Chris Abratte of the Cornell Stem Cell and Transgenic Core Facility. This work was supported by the Cornell Center for Vertebrate Genomics (I.C.W.), NIH institutional support for I.C.W. (HD057854), and NIH R01 DK092776 (N.A.K.).

Received: April 9, 2015
Revised: July 20, 2015
Accepted: August 24, 2015
Published: September 24, 2015

REFERENCES

Almada, A.E., Wu, X., Kriz, A.J., Burge, C.B., and Sharp, P.A. (2013). Promoter directionality is controlled by U1 snRNP and polyadenylation signals. Nature *499*, 360–363.

Core, L.J., Waterfall, J.J., and Lis, J.T. (2008). Nascent RNA sequencing reveals widespread pausing and divergent initiation at human promoters. Science *322*, 1845–1848.

Core, L.J., Martins, A.L., Danko, C.G., Waters, C.T., Siepel, A., and Lis, J.T. (2014). Analysis of nascent RNA identifies a unified architecture of initiation regions at mammalian promoters and enhancers. Nat. Genet. *46*, 1311–1320.

Creyghton, M.P., Cheng, A.W., Welstead, G.G., Kooistra, T., Carey, B.W., Steine, E.J., Hanna, J., Lodato, M.A., Frampton, G.M., Sharp, P.A., et al. (2010). Histone H3K27ac separates active from poised enhancers and predicts developmental state. Proc. Natl. Acad. Sci. USA *107*, 21931–21936.

Danko, C.G., Hyland, S.L., Core, L.J., Martins, A.L., Waters, C.T., Lee, H.W., Cheung, V.G., Kraus, W.L., Lis, J.T., and Siepel, A. (2014). Accurate identification of active transcriptional regulatory elements from global run-on and sequencing data. bioRxiv. http://www.biorxiv.org/content/early/2014/11/12/011353.

Davis, N.M., Kurpios, N.A., Sun, X., Gros, J., Martin, J.F., and Tabin, C.J. (2008). The chirality of gut rotation derives from left-right asymmetric changes in the architecture of the dorsal mesentery. Dev. Cell *15*, 134–145.

de Wit, E., and de Laat, W. (2012). A decade of 3C technologies: insights into nuclear organization. Genes Dev. *26*, 11–24.

Dixon, J.R., Selvaraj, S., Yue, F., Kim, A., Li, Y., Shen, Y., Hu, M., Liu, J.S., and Ren, B. (2012). Topological domains in mammalian genomes identified by analysis of chromatin interactions. Nature *485*, 376–380.

Dowen, J.M., Fan, Z.P., Hnisz, D., Ren, G., Abraham, B.J., Zhang, L.N., Weintraub, A.S., Schuijers, J., Lee, T.I., Zhao, K., and Young, R.A. (2014). Control of cell identity genes occurs in insulated neighborhoods in mammalian chromosomes. Cell *159*, 374–387.

Duboc, V., Röttinger, E., Lapraz, F., Besnardeau, L., and Lepage, T. (2005). Left-right asymmetry in the sea urchin embryo is regulated by nodal signaling on the right side. Dev. Cell *9*, 147–158.

Flomen, R.H., Vatcheva, R., Gorman, P.A., Baptista, P.R., Groet, J., Barisić, I., Ligutic, I., and Nizetić, D. (1998). Construction and analysis of a sequence-ready map in 4q25: Rieger syndrome can be caused by haploinsufficiency of RIEG, but also by chromosome breaks approximately 90 kb upstream of this gene. Genomics *47*, 409–413.

Franco, D., and Campione, M. (2003). The role of Pitx2 during cardiac development. Linking left-right signaling and congenital heart diseases. Trends Cardiovasc. Med. *13*, 157–163.

Grote, P., and Herrmann, B.G. (2013). The long non-coding RNA Fendrr links epigenetic control mechanisms to gene regulatory networks in mammalian embryogenesis. RNA Biol. *10*, 1579–1585.

Grote, P., Wittler, L., Hendrix, D., Koch, F., Währisch, S., Beisaw, A., Macura, K., Bläss, G., Kellis, M., Werber, M., and Herrmann, B.G. (2013). The tissue-specific lncRNA Fendrr is an essential regulator of heart and body wall development in the mouse. Dev. Cell *24*, 206–214.

Hamburger, V., and Hamilton, H.L. (1951). A series of normal stages in the development of the chick embryo. J. Morphol. *88*, 49–92.

Hamburger, V., and Hamilton, H.L. (1992). A series of normal stages in the development of the chick embryo. 1951. Dev. Dyn. *195*, 231–272.

Hsu, P.D., Scott, D.A., Weinstein, J.A., Ran, F.A., Konermann, S., Agarwala, V., Li, Y., Fine, E.J., Wu, X., Shalem, O., et al. (2013). DNA targeting specificity of RNA-guided Cas9 nucleases. Nat. Biotechnol. *31*, 827–832.

Johnsson, P., Lipovich, L., Grandér, D., and Morris, K.V. (2014). Evolutionary conservation of long non-coding RNAs; sequence, structure, function. Biochim. Biophys. Acta *1840*, 1063–1071.

Kagey, M.H., Newman, J.J., Bilodeau, S., Zhan, Y., Orlando, D.A., van Berkum, N.L., Ebmeier, C.C., Goossens, J., Rahl, P.B., Levine, S.S., et al. (2010). Mediator and cohesin connect gene expression and chromatin architecture. Nature *467*, 430–435.

Kampstra, P. (2008). Beanplot: a boxplot alternative for visual comparison of distributions. J. Stat. Softw. *28*, 1–9.

Kent, W.J., Sugnet, C.W., Furey, T.S., Roskin, K.M., Pringle, T.H., Zahler, A.M., and Haussler, D. (2002). The human genome browser at UCSC. Genome Res. *12*, 996–1006.

Kikuta, H., Laplante, M., Navratilova, P., Komisarczuk, A.Z., Engström, P.G., Fredman, D., Akalin, A., Caccamo, M., Sealy, I., Howe, K., et al. (2007). Genomic regulatory blocks encompass multiple neighboring genes and maintain conserved synteny in vertebrates. Genome Res. *17*, 545–555.

Kurpios, N.A., Ibañes, M., Davis, N.M., Lui, W., Katz, T., Martin, J.F., Izpisúa Belmonte, J.C., and Tabin, C.J. (2008). The direction of gut looping is established by changes in the extracellular matrix and in cell:cell adhesion. Proc. Natl. Acad. Sci. USA *105*, 8499–8506.

Kurz, A., Lampel, S., Nickolenko, J.E., Bradl, J., Benner, A., Zirbel, R.M., Cremer, T., and Lichter, P. (1996). Active and inactive genes localize preferentially in the periphery of chromosome territories. J. Cell Biol. *135*, 1195–1205.

Liu, C., Liu, W., Lu, M.F., Brown, N.A., and Martin, J.F. (2001). Regulation of left-right asymmetry by thresholds of Pitx2c activity. Development *128*, 2039–2048.

Logan, M., Pagán-Westphal, S.M., Smith, D.M., Paganessi, L., and Tabin, C.J. (1998). The transcription factor Pitx2 mediates situs-specific morphogenesis in response to left-right asymmetric signals. Cell *94*, 307–317.

Lu, M.F., Pressman, C., Dyer, R., Johnson, R.L., and Martin, J.F. (1999). Function of Rieger syndrome gene in left-right asymmetry and craniofacial development. Nature *401*, 276–278.

Lubitz, S.A., Sinner, M.F., Lunetta, K.L., Makino, S., Pfeufer, A., Rahman, R., Veltman, C.E., Barnard, J., Bis, J.C., Danik, S.P., et al. (2010). Independent susceptibility markers for atrial fibrillation on chromosome 4q25. Circulation *122*, 976–984.

Mahadevan, A., Welsh, I.C., Sivakumar, A., Gludish, D.W., Shilvock, A.R., Noden, D.M., Huss, D., Lansford, R., and Kurpios, N.A. (2014). The left-right Pitx2 pathway drives organ-specific arterial and lymphatic development in the intestine. Dev. Cell *31*, 690–706.

Marinić, M., Aktas, T., Ruf, S., and Spitz, F. (2013). An integrated holo-enhancer unit defines tissue and gene specificity of the Fgf8 regulatory landscape. Dev. Cell *24*, 530–542.

Melgar, M.F., Collins, F.S., and Sethupathy, P. (2011). Discovery of active enhancers through bidirectional expression of short transcripts. Genome Biol. *12*, R113.

Nitsche, A., Rose, D., Fasold, M., Reiche, K., and Stadler, P.F. (2015). Comparison of splice sites reveals that long noncoding RNAs are evolutionarily well conserved. RNA *21*, 801–812.

Nobrega, M.A., Ovcharenko, I., Afzal, V., and Rubin, E.M. (2003). Scanning human gene deserts for long-range enhancers. Science *302*, 413.

Nora, E.P., Dekker, J., and Heard, E. (2013). Segmental folding of chromosomes: a basis for structural and regulatory chromosomal neighborhoods? BioEssays *35*, 818–828.

Phillips-Cremins, J.E., Sauria, M.E.G., Sanyal, A., Gerasimova, T.I., Lajoie, B.R., Bell, J.S.K., Ong, C.T., Hookway, T.A., Guo, C., Sun, Y., et al. (2013). Architectural protein subclasses shape 3D organization of genomes during lineage commitment. Cell *153*, 1281–1295.

Reis, L.M., Tyler, R.C., Volkmann Kloss, B.A., Schilter, K.F., Levin, A.V., Lowry, R.B., Zwijnenburg, P.J.G., Stroh, E., Broeckel, U., Murray, J.C., and Semina, E.V. (2012). PITX2 and FOXC1 spectrum of mutations in ocular syndromes. Eur. J. Hum. Genet. *20*, 1224–1233.

Rinn, J.L., and Chang, H.Y. (2012). Genome regulation by long noncoding RNAs. Annu. Rev. Biochem. *81*, 145–166.

Ruf, S., Symmons, O., Uslu, V.V., Dolle, D., Hot, C., Ettwiller, L., and Spitz, F. (2011). Large-scale analysis of the regulatory architecture of the mouse genome with a transposon-associated sensor. Nat. Genet. *43*, 379–386.

Semina, E.V., Reiter, R., Leysens, N.J., Alward, W.L., Small, K.W., Datson, N.A., Siegel-Bartelt, J., Bierke-Nelson, D., Bitoun, P., Zabel, B.U., et al. (1996). Cloning and characterization of a novel bicoid-related homeobox transcription factor gene, RIEG, involved in Rieger syndrome. Nat. Genet. *14*, 392–399.

Shen, Y., Yue, F., McCleary, D.F., Ye, Z., Edsall, L., Kuan, S., Wagner, U., Dixon, J., Lee, L., Lobanenkov, V.V., and Ren, B. (2012). A map of the cis-regulatory sequences in the mouse genome. Nature *488*, 116–120.

Shiratori, H., Sakuma, R., Watanabe, M., Hashiguchi, H., Mochida, K., Sakai, Y., Nishino, J., Saijoh, Y., Whitman, M., and Hamada, H. (2001). Two-step regulation of left-right asymmetric expression of Pitx2: initiation by nodal signaling and maintenance by Nkx2. Mol. Cell *7*, 137–149.

Shiratori, H., Yashiro, K., Shen, M.M., and Hamada, H. (2006). Conserved regulation and role of Pitx2 in situs-specific morphogenesis of visceral organs. Development *133*, 3015–3025.

Shiratori, H., Yashiro, K., Iwai, N., Oki, S., Minegishi, K., Ikawa, Y., Kanata, K., and Hamada, H. (2014). Self-regulated left-right asymmetric expression of Pitx2c in the developing mouse limb. Dev. Biol. *395*, 331–341.

Splinter, E., Heath, H., Kooren, J., Palstra, R.J., Klous, P., Grosveld, F., Galjart, N., and de Laat, W. (2006). CTCF mediates long-range chromatin looping and local histone modification in the beta-globin locus. Genes Dev. *20*, 2349–2354.

Tao, Y., Zhang, M., Li, L., Bai, Y., Zhou, Y., Moon, A.M., Kaminski, H.J., and Martin, J.F. (2014). Pitx2, an atrial fibrillation predisposition gene, directly regulates ion transport and intercalated disc genes. Circ Cardiovasc Genet *7*, 23–32.

Trask, B.J., Massa, H., Kenwrick, S., and Gitschier, J. (1991). Mapping of human chromosome Xq28 by two-color fluorescence in situ hybridization of DNA sequences to interphase cell nuclei. Am. J. Hum. Genet. *48*, 1–15.

Vance, K.W., and Ponting, C.P. (2014). Transcriptional regulatory functions of nuclear long noncoding RNAs. Trends Genet. *30*, 348–355.

Visel, A., Minovitsky, S., Dubchak, I., and Pennacchio, L.A. (2007). VISTA Enhancer Browser–a database of tissue-specific human enhancers. Nucleic Acids Res. *35*, D88–D92.

Volkmann, B.A., Zinkevich, N.S., Mustonen, A., Schilter, K.F., Bosenko, D.V., Reis, L.M., Broeckel, U., Link, B.A., and Semina, E.V. (2011). Potential novel mechanism for Axenfeld-Rieger syndrome: deletion of a distant region containing regulatory elements of PITX2. Invest. Ophthalmol. Vis. Sci. *52*, 1450–1459.

Waite, M.R., Skidmore, J.M., Micucci, J.A., Shiratori, H., Hamada, H., Martin, J.F., and Martin, D.M. (2013). Pleiotropic and isoform-specific functions for Pitx2 in superior colliculus and hypothalamic neuronal development. Mol. Cell. Neurosci. *52*, 128–139.

Wang, J., Bai, Y., Li, N., Ye, W., Zhang, M., Greene, S.B., Tao, Y., Chen, Y., Wehrens, X.H.T., and Martin, J.F. (2014). Pitx2-microRNA pathway that delimits sinoatrial node development and inhibits predisposition to atrial fibrillation. Proc. Natl. Acad. Sci. USA *111*, 9181–9186.

Watanabe, H., Schmidt, H.A., Kuhn, A., Höger, S.K., Kocagöz, Y., Laumann-Lipp, N., Ozbek, S., and Holstein, T.W. (2014). Nodal signalling determines biradial asymmetry in Hydra. Nature *515*, 112–115.

Welsh, I.C., Thomsen, M., Gludish, D.W., Alfonso-Parra, C., Bai, Y., Martin, J.F., and Kurpios, N.A. (2013). Integration of left-right Pitx2 transcription and Wnt signaling drives asymmetric gut morphogenesis via Daam2. Dev. Cell *26*, 629–644.

West, A.G., Gaszner, M., and Felsenfeld, G. (2002). Insulators: many functions, many mechanisms. Genes Dev. *16*, 271–288.